Cellular Signalling 27 (2015) 978–988

Contents lists available at ScienceDirect

Cellular Signalling

journal homepage: www.elsevier.com/locate/cellsig

Motif affinity and mass spectrometry proteomic approach for the discovery of cellular AMPK targets: Identification of mitochondrial fission factor as a new AMPK substrate

Serge Ducommun [a,b], Maria Deak [a], David Sumpton [c], Rebecca J. Ford [d], Antonio Núñez Galindo [a], Martin Kussmann [a,b], Benoit Viollet [e,f,g], Gregory R. Steinberg [d], Marc Foretz [e,f,g], Loïc Dayon [a], Nicholas A. Morrice [c,1], Kei Sakamoto [a,b,*]

[a] Nestlé Institute of Health Sciences SA, EPFL Innovation Park, bâtiment G/H, 1015 Lausanne, Switzerland
[b] School of Life Sciences, Ecole Polytechnique Fédérale de Lausanne (EPFL), 1015 Lausanne, Switzerland
[c] Beatson Institute for Cancer Research, Bearsden, Glasgow G61 1BD, UK
[d] Department of Medicine, Division of Endocrinology and Metabolism, McMaster University, Hamilton, Ontario, Canada
[e] Inserm, U1016, Institut Cochin, Paris, France
[f] CNRS, UMR 8104, Paris, France
[g] Université Paris Descartes, Sorbonne Paris cité, Paris, France

ARTICLE INFO

Article history:
Received 27 January 2015
Accepted 8 February 2015
Available online 13 February 2015

Keywords:
Energy metabolism
Protein kinase
Cell signalling
Mitochondrial dynamics
Mitochondrial fission

ABSTRACT

AMP-activated protein kinase (AMPK) is a key cellular energy sensor and regulator of metabolic homeostasis. Although it is best known for its effects on carbohydrate and lipid metabolism, AMPK is implicated in diverse cellular processes, including mitochondrial biogenesis, autophagy, and cell growth and proliferation. To further our understanding of energy homeostasis through AMPK-dependent processes, the design and application of approaches to identify and characterise novel AMPK substrates are invaluable. Here, we report an affinity proteomicstrategy for the discovery and validation of AMPK targets using an antibody to isolate proteins containing the phospho-AMPK substrate recognition motif from hepatocytes that had been treated with pharmacological AMPK activators. We identified 57 proteins that were uniquely enriched in the activator-treated hepatocytes, but were absent in hepatocytes lacking AMPK. We focused on two candidates, cingulin and mitochondrial fission factor (MFF), and further characterised/validated them as AMPK-dependent targets by immunoblotting with phosphorylation site-specific antibodies. A small-molecule AMPK activator caused transient phosphorylation of endogenous cingulin at S137 in intestinal Caco2 cells. Multiple splice-variants of MFF appear to express in hepatocytes and we identified a common AMPK-dependent phospho-site (S129) in all the 3 predominant variants spanning the mass range and a short variant-specific site (S146). Collectively, our proteomic-based approach using a phospho-AMPK substrate antibody in combination with genetic models and selective AMPK activators will provide a powerful and reliable platform for identifying novel AMPK-dependent cellular targets.

1. Introduction

Maintaining the balance of ATP-generating and ATP-consuming processes is a fundamental component of cellular energy homeostasis. AMP-activated protein kinase (AMPK) is a central energy/nutrient sensor of adenine nucleotide levels that is stimulated when cells/tissues are exposed to metabolic stresses (e.g. hypoxia, ischaemia) that lower cellular energy status by decreasing the catabolic generation of ATP or by promoting ATP consumption (e.g. muscle contraction). In response, AMPK functions to restore energy homeostasis by slowing the rate of anabolic pathways and other ATP-consuming processes while accelerating ATP-producing catabolic pathways.

AMPK is a heterotrimer comprising a catalytic α subunit and regulatory β and γ subunits. Multiple isoforms encoded by distinct genes exist (α1, α2; β1, β2; γ1, γ2, γ3), which can form multiple distinct heterotrimeric combinations [1,2]. The γ subunits contain four tandem cystathionine β-synthase (CBS) repeats that impart adenine nucleotide binding. AMPK activity increases upon phosphorylation of a conserved

Abbreviations: AMPK, 5′-AMP-activated protein kinase; ACC, acetyl-CoA carboxylase; HMGCR, 3-hydroxy-3-methyl-glutaryl-CoA reductase; TBC1D1, TBC1 (tre-2/USP6, BUB2, cdc16) domain family member 1; ZO, zonula occludens.

* Corresponding author at: Nestlé Institute of Health Sciences SA, EPFL Innovation Park, bâtiment G, 1015 Lausanne, Switzerland. Tel.: +41 216326133; fax: +41 216326499.
E-mail address: Kei.Sakamoto@rd.nestle.com (K. Sakamoto).
[1] Current address: AB-Sciex, Phoenix House, Centre Park, Warrington WA1 1RX, UK.

http://dx.doi.org/10.1016/j.cellsig.2015.02.008

threonine residue within the activation loop (T172) [1]. Binding of ADP and/or AMP induces conformational changes that promote net T172 phosphorylation by (1) the enhancement of T172 phosphorylation and (2) the suppression of T172 dephosphorylation [3–5]. In addition, the binding of AMP (but not ADP) further increases AMPK activity by direct allosteric activation [3]. The major upstream kinase phosphorylating T172 in most mammalian cells is a complex containing LKB1, which itself seems to be constitutively active [6,7]. In some cellular environs, T172 can be phosphorylated in a Ca^{2+}-mediated process catalysed by Ca^{2+}/calmodulin-dependent protein kinase kinases [1,2].

AMPK is considered an important future target for drugs to treat metabolic disorders, as AMPK activation brings about metabolic responses desirable to counteract the metabolic abnormalities associated with obesity, insulin resistance, and type 2 diabetes. For instance, AMPK phosphorylates and inactivates acetyl-CoA carboxylase-1 (ACC1) and 3-hydroxy-3-methyl-glutaryl-CoA reductase (HMGCR), key enzymes of fatty acid and sterol biosynthesis, respectively. Moreover, previous studies have demonstrated that the activation of AMPK promotes fatty acid oxidation through phosphorylation of acetyl-CoA carboxylase-2 (ACC2) and glucose uptake in skeletal muscle involving phosphorylation of TBC1D1 [1,2,8–11].

Although it is best known for its effects on metabolism, AMPK is implicated in many other processes, including mitochondrial biogenesis and disposal, autophagy, cell polarity, and cell growth and proliferation [12]. To deepen our understanding of cellular energy homeostasis through AMPK-dependent processes, development and application of approaches to identify novel AMPK substrates are important. Previous studies have elucidated the AMPK recognition motif by employing multiple approaches, including synthetic peptides [13], site-directed mutagenesis with a recombinant substrate and molecular modelling [14,15], and more recently a peptide library approach [16]. AMPK phosphorylates sites that have at least one basic side chain (usually R, but can be K or H) either four or three residues N-terminal with respect to the phospho-acceptor site (S or T). It also requires hydrophobic side chains at −5 and +4 (usually L or M, but I, V or F in some cases) [12]. We sought to take advantage of this established AMPK substrate motif by utilising an antibody raised against a degenerate peptide library containing fixed leucine and arginine residues at the −5 and −3 positions N-terminal to the phospho-acceptor (S/T) residue to immunoprecipitate and identify potential AMPK substrates by mass spectrometry (MS). Here we report a list of potential cellular AMPK targets and validation/biochemical characterisation of two selected hits, cingulin and mitochondrial fission factor (MFF).

2. Materials and methods

2.1. Materials

Materials used include λ-phosphatase (P0753; New England Biolabs), 5-aminoimidazole-4-carboxamide riboside (AICAR, A611700; Toronto Research Chemicals), mass spectrometry grade trypsin (V528A; Promega), Protein G Sepharose (P3296; Sigma), FLAG-M2 resin (A2220; Sigma) and NHS-activated Sepharose (17-0906-01; GE Healthcare). A769662 was synthesized as described previously [17] or obtained from Selleck Chemicals (S2697). 991 (5-[[6-chloro-5-(1-methylindol-5-yl)-1H-benzimidazol-2-yl]oxy]-2-methyl-benzoic acid) (CAS#: 129739-36-2) was synthesized by Spirochem. COS-1 (CRL-1650) and Caco2 (HTB-37) cell lines were obtained from ATCC. General and specific cell culture reagents, including Williams' medium E, were obtained from Life Technologies. Formic acid (FA, 99%) and acetonitrile were from BDH. Water (18.2 MΩ·cm at 25 °C) was obtained from a Milli-Q apparatus (Millipore). All other materials unless otherwise indicated were from Sigma.

2.2. Antibodies

Total acetyl-CoA carboxylase (ACC; #3676), phospho-ACC1 (S79; #3661), total Raptor (#2280), phospho-Raptor (S792; #2083), total AMPKα (#2532), phospho-AMPKα (T172; #2535), total p70 S6 kinase (p70S6K; #2708) and phospho-p70S6K (T389; #9234) and phospho-(S/T) AMPK substrate motif (#5759, lot #4) antibodies were from Cell Signaling Technology. Total mitochondrial fission factor (MFF) antibodies were from Proteintech (17090-1-AP) and Santa Cruz Biotechnology (sc-168593). Total cingulin antibodies were from Proteintech (21369-1-AP) and Santa Cruz Biotechnology (sc-365264). The antibodies against α-tubulin (T6074) and FLAG (F7425) were from Sigma. Horseradish peroxidase-conjugated secondary antibodies were from Jackson ImmunoResearch Europe. Site-specific rabbit polyclonal antibodies against phospho-MFF and phospho-cingulin were generated by YenZym Antibodies (South San Francisco, CA, USA) by immunisation with a phosphorylated peptide of the human sequence (CRLKRER-*S-MSENAVR-amide for pS129 MFF, CKRERSM-*S-ENAVRQN-amide for pS131 MFF, CGQLVRND-*S-MYGISN-amide for pS146 MFF and the prefix * denotes the phosphorylated residue) or a combination of two phosphorylated peptides of the human and mouse sequences (CKLLRSH-*S-QASLAGP-amide and CKLIRSQ-*S-QASLTGL-amide for pS137 cingulin).

2.3. Animals

Wild-type male C57BL/6 mice were obtained from Jackson Laboratories. All protocols for animal use and euthanasia were approved by the McMaster University Animal Research Ethics Board. Generation of liver-specific AMPKα1/α2 knockout mice has been described previously [18]. Experiments using AMPKα1/α2 double knockout and its control mice were performed under the approval of the ethics committee from University Paris Descartes (no. CEEA34.BV.157.12) and the French authorisation to experiment on vertebrates (no. 75-886) in accordance with the European guidelines.

2.4. Cloning and mutagenesis

The coding regions of cDNAs of interest were generated using the GoTaq 1-step PCR system (Promega). Human cingulin (NM_020770.2) was amplified from human pancreas RNA (Agilent, 540023). Mouse MFF amplification primers were designed based on sequence NM_029409.2 (Forward primer: 5′-GGATCCATGGCAGAAATTAGTCGAATTCAGTA-3′, reverse primer: 5′-CTAGCGTCGAAACCAGAGCCAGCTGT-3′). RNA from 5 different mouse tissues (brain, 736001; heart, 736005; kidney, 736007; liver, 736009; and testis, 736023; all from Agilent) was used as a template. The resulting PCR products were ligated into intermediate vectors using Strataclone PCR cloning kit (Agilent). Site-directed mutagenesis was performed according to the QuikChange method (Stratagene) using KOD polymerase (Novagen). The sequences of all the clones have been verified utilising the BigDye Terminator 3.1 kit and 3500XL Genetic analyzer (Applied Biosystems) in-house at Nestlé Institute of Health Sciences.

2.5. General cell culture and mouse primary hepatocytes

Caco2 cells were cultured in DMEM supplemented with 15% foetal calf serum and 1× MEM non-essential amino acids. Experiments were performed on cells cultured for 2 days after reaching confluence. COS-1 cells were cultured in DMEM supplemented with 10% foetal calf serum. Cells were transfected with DNA using polyethylenimine, treated and harvested 36 h post-transfection. Cells were washed with ice-cold PBS and scraped into lysis buffer (50 mM tris pH 7.5, 1 mM EDTA, 1 mM EGTA, 0.27 M sucrose, 1% (w/v) Triton X-100, 20 mM glycerol-2-phosphate, 50 mM NaF, 5 mM sodium pyrophosphate, 0.5 mM PMSF, 1 mM benzamidine, 1 mM dithiothreitol, 1 mM

Na_3VO_4). Primary hepatocytes were isolated by collagenase perfusion and cultured as previously described [18–20]. Cells were treated with or without AICAR and A769662 as indicated in figure legends. Following the treatment, media were aspirated and cells lysed on ice in cold lysis buffer containing 1% complete protease inhibitor cocktail (Roche). Lysates were snap-frozen in liquid nitrogen and stored at −80 °C for subsequent analyses. Lysates were clarified at 3500 g for 15 min at 4 °C and normalised using Bradford reagent and BSA as standard.

2.6. Immunoprecipitation, phosphatase treatment and immunoblotting

For immunoprecipitation, lysates were incubated with 1 μg of antibody and 5 μl of Protein G Sepharose or 5 μl FLAG-M2 resin on a vibrating platform shaker (1000 rpm) for 2 h at 4 °C. For immunoprecipitation of MFF from cell extracts, the antibody was cross-linked to NHS-activated Sepharose according to the manufacturer's instructions. Dephosphorylation of overexpressed protein was performed as previously described [21]. Briefly, FLAG-MFF was immunoprecipitated using FLAG-M2 resin and dephosphorylated using λ-phosphatase for 30 min at 30 °C. Dephosphorylation reactions were terminated by denaturation in Laemmli buffer and samples were separated by SDS-PAGE, and transferred to nitrocellulose membrane. Membranes were blocked for 1 h in 20 mM tris (pH 7.6), 137 mM NaCl, 0.1% (v/v) Tween-20 (TBST) containing 5% (w/v) skimmed milk. Membranes were incubated in primary antibody prepared in TBST containing 1% (w/v) BSA overnight at 4 °C. Detection was performed using horseradish peroxidase-conjugated secondary antibodies and enhanced chemiluminescence reagent.

2.7. Trypsin digestion and MS analysis

Immunoprecipitated proteins from hepatocyte lysates (2 mg) were denatured in Laemmli buffer, alkylated using iodoacetamide and separated by SDS-PAGE on NuPAGE 4–12% bis-tris gels (Life Technologies). Gels were stained with colloidal Coomassie and regions of interest were excised. Gel pieces were destained by successive washing (10 min, 30 °C) in water, 50% acetonitrile, 0.1 M triethylammonium bicarbonate (TEAB, pH 8.5) and 50 mM TEAB in 50% acetonitrile. Gel pieces were dehydrated in 100% acetonitrile and dried by Speedvac before rehydration in 25 mM TEAB containing 5 μg/ml trypsin overnight (30 °C). The peptide digestion products were then extracted sequentially with one volume of 100% acetonitrile (15 min, 30 °C) and one volume of 25% acetonitrile and 1.25% formic acid (15 min, 30 °C). The resulting supernatants were pooled and evaporated. Dried peptides were redissolved in 5% acetonitrile/0.25% formic acid. Reversed-phase liquid chromatography tandem MS (RPLC-MS/MS) analysis was performed on a LTQ-Orbitrap Velos coupled to a Proxeon Easy-LC. The peptide mixtures were loaded onto a C_{18} guard column (1.9 μm; 0.1 × 20 mm) and separated on a C_{18} in-house packed emitter (1.9 μm; 0.075 × 150 mm) over a 55 min linear gradient (5% to 45% B. A: 2% acetonitrile 0.1% formic acid B: 80% acetonitrile 0.1% formic acid). The Orbitrap was set to analyse the survey scans (m/z 350 to 1600) at 60,000 resolution and the top 10 ions in each duty cycle were selected for MS/MS in the LTQ linear ion trap with collision-induced dissociation (CID) (normalised collision energy (NCE) 36%). The data was searched against the Swiss-Prot database (26/01/2014 release) restricted to *Mus musculus* (16656 entries) using Mascot (2.4.1). All Mascot result files were loaded into Scaffold (4.3.4). Peptide and protein thresholds were set to 95.0% with a 2 unique peptide criterion to report protein identification.

For analysis of MFF sites phosphorylated in vivo, dried peptides were dissolved in 3% acetonitrile/0.1% formic acid. RPLC-MS/MS analysis was performed on a LTQ-Orbitrap Elite equipped with an Ultimate 3000 RSLC nano system. The analytical separation was run for 70 min using an Acclaim PepMap RSLC 75 μm × 50 cm (C18, 2 μm, 100 Å) column. For survey scans, the Orbitrap resolution was 120,000 with an m/z window from 300 to 1500. The top 20 precursor ions were selected for MS/MS in the LTQ with CID (NCE 30%). The data was searched against the Q6PCP5-4|MFF_MOUSE sequence from Swiss-Prot (07/03/2014 release) using Mascot (2.4.0). All Mascot result files were loaded into Scaffold (4.3.2). Peptide and protein thresholds were 95.0% and 99.0% respectively with a 2 unique peptide criterion.

3. Results

3.1. Immunoprecipitation and identification of AMPK-regulated/phosphorylated proteins in hepatocytes utilising the phospho-AMPK substrate motif antibody and MS

Mouse primary hepatocytes were treated with a combination of two pharmacological AMPK activators, AICAR (0.3 mM) and A769662 (10 μM), which causes an acute and robust activation of AMPK compared to single compound treatment [18,21]. Immunoblot analysis of total cell extracts confirmed a potent activation of AMPK in the compound-treated samples, as phosphorylation of AMPKα within the activation loop (T172) as well as phosphorylation of known bona fide AMPK substrates (ACC and Raptor) was markedly increased (Fig. 1A). We also observed that the treated samples showed a robust inhibition of p70S6K phosphorylation (T389), a well characterised consequence of AMPK activation due to suppression of mTOR complex 1 by phosphorylation of Raptor and tuberous sclerosis 2 (TSC2 (also known as tuberin)) [1] (Fig. 1A). Immunoblotting of the hepatocyte extracts with the phospho-AMPK substrate motif antibody demonstrated that the antibody readily recognised several protein bands at various molecular weights in the untreated samples, and overall number and intensity of the bands were substantially increased upon treatment (Fig. 1A).

In order to identify the proteins that were immunoreactive with the phospho-AMPK motif antibody, total hepatocyte extracts (that had been treated with or without the AMPK activator cocktail) were immunoprecipitated with the phospho-AMPK substrate motif antibody or rabbit IgG (non-specific control) and the resulting immunoprecipitates were subjected to SDS-PAGE, in-gel tryptic digestion followed by MS/MS analysis. A Coomassie-stained gel of the immunoprecipitates showed that although several unique (absent in the IgG control) protein bands were present in the samples immunoprecipitated with the phospho-AMPK motif antibody, only a small minority were enriched in the treated samples (indicated with asterisk in Fig. 1B). Possible reasons for such a modest difference between the treated and the untreated group (as compared to the phospho-AMPK motif immunoblot of the total extract in Fig. 1A) could be that AMPK-activator-regulated bands might have been masked by non-specific bands or the abundance of the regulated bands was too low to be detected by Coomassie staining. Another reason could be that as the phospho-AMPK motif antibody was raised against a short linear peptide, it will not recognise all the phospho-sites in folded native proteins.

Tryptic peptides derived from the experiment shown in Fig. 1B were analysed by LC-MS/MS and the resulting data were searched against the Swiss-Prot mouse database. To demonstrate consistency and reproducibility of the analysis a technical replicate (immunoprecipitation plus LC-MS/MS) using the same hepatocyte lysates was performed (exp1a and exp1b). A total of 549 proteins were detected (2 peptides minimum with 95% probability) across both runs. After removing proteins present in the IgG negative control, we performed label-free quantification by total spectral counting. 99 proteins were enriched in the treated versus untreated samples in the first run (exp1a). In the second run (exp1b), 59 enriched proteins were identified, of which the vast majority were also present in the first run (Fig. 1C). In total, 101 proteins were enriched in the treated versus untreated samples (Fig. 1C). We then performed a biological replicate (independent isolation of primary hepatocytes; 776 proteins detected with 2 peptides minimum and

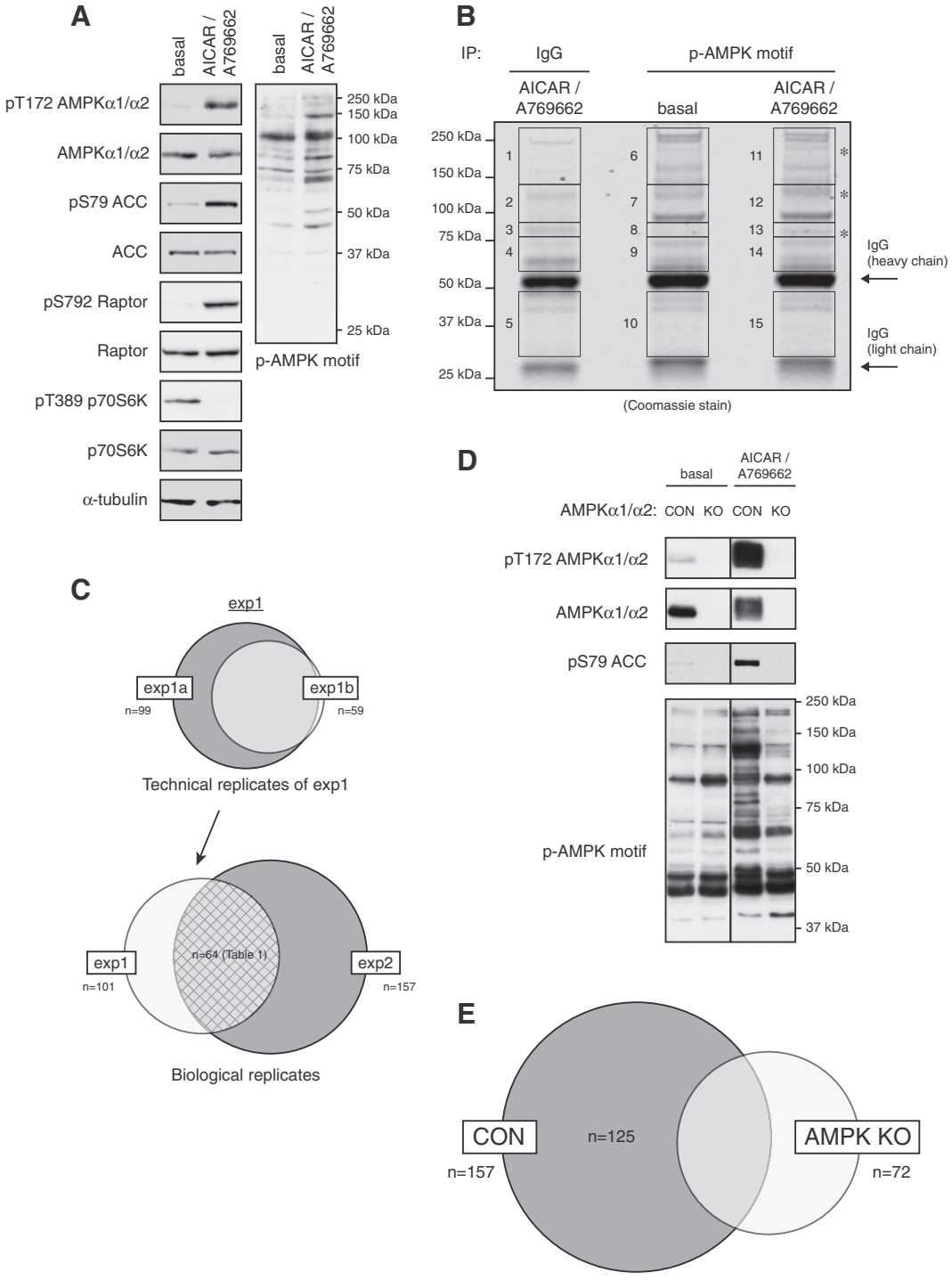

Fig. 1. Analysis of phospho-AMPK substrate motif antibody immunoprecipitates by MS/MS. (A, B) Primary hepatocytes were isolated from male C57BL/6 mice (12-week-old). Hepatocytes were incubated with vehicle or a combination of 0.3 mM AICAR and 10 μM A769662 for 45 min. (A) Cell lysates (20 μg) were analysed by immunoblotting using the indicated antibodies. (B) Total cell lysates (2 mg) were immunoprecipitated using 1 μg anti-phospho-AMPK-substrate motif (p-AMPK motif) or non-specific control rabbit antibody (IgG). Immunoprecipitates were separated by SDS-PAGE and the gel was stained using colloidal Coomassie. Boxes on the image indicate where gel bands were excised for subsequent sample processing (trypsin digestion and MS/MS analysis). (C) Samples from panel B were analysed by LC-MS/MS, searched against the Swiss-Prot mouse database and the amount of protein detected was quantified by total spectral counting. 99 proteins were enriched in the stimulated versus basal samples in the first run (exp1a) and 59 in the technical replicate using the same starting material (exp1b) (upper diagram). In total, 101 proteins were enriched in the stimulated versus basal samples (exp1). In a biological replicate of the experiment, 157 proteins were enriched in the stimulated versus basal samples (exp2). Across both biological replicates, 64 proteins were enriched (lower diagram). (D) Primary hepatocytes were isolated from AMPKα1/α2 liver-specific knockout mice (KO) and AMPKα1$^{lox/lox}$α2$^{lox/lox}$ mice (CON) (10-week-old). Plated cells were treated with vehicle or a combination of 0.3 mM AICAR and 10 μM A769662 for 45 min. Cell extracts (20 μg) were analysed by immunoblot analysis using the indicated antibodies. (E) Primary hepatocytes from control and AMPK KO mice were treated with vehicle or a combination of 0.3 mM AICAR and 10 μM A769662 for 45 min. Total cell lysates (2 mg) were immunoprecipitated using anti-phospho-AMPK motif antibody (p-AMPK motif) or control rabbit IgG. Immunoprecipitates were separated by SDS-PAGE and the gel was stained using colloidal Coomassie. Regions of the gel (analogous to panel B) were excised (image not shown) for further processing (trypsin digestion and MS/MS analysis). 72 proteins were enriched upon stimulation in the sample originating from AMPK KO, and 157 proteins in the sample from control mouse hepatocytes (CON). 125 proteins were uniquely enriched in the control sample.

Table 1
List of potential AMPK substrates/targets identified by MS analysis (Fig. 1B and C). Known AMPK substrates are highlighted in green. Proteins that did not fulfil the criteria of AMPK dependent regulation (Fig. 1E) are greyed out at the bottom of the list.

Accession	Gene name	Protein name
Q8CBW3	Abi1	Abl interactor 1
Q8K4G5	Ablim1	Actin-binding LIM protein 1
Q5SWU9	Acaca	Acetyl-CoA carboxylase 1
Q8VHH5	Agap3	Arf-GAP with GTPase, ANK repeat and PH domain-containing protein 3
O08739	Ampd3	AMP deaminase 3
Q3UMR0	Ankrd27	Ankyrin repeat domain-containing protein 27
Q7TPS5	C2cd5	C2 domain-containing protein 5
Q80U49	Cep170b	Centrosomal protein of 170 kDa protein B
P59242	Cgn	Cingulin
Q68FD5	Cltc	Clathrin heavy chain 1
Q3UMF0	Cobll1	Cordon-bleu protein-like 1
Q7TMB8	Cyfip1	Cytoplasmic FMR1-interacting protein 1
P11531	Dmd	Dystrophin
E9Q557	Dsp	Desmoplakin
Q80TH2	Erbb2ip	Protein LAP2
Q3UQN2	Fcho2	FCH domain only protein 2
Q9JI19	Fibp	Acidic fibroblast growth factor intracellular-binding protein
Q9Z1S8	Gab2	GRB2-associated-binding protein 2
Q6PAR5	Gapvd1	GTPase-activating protein and VPS9 domain-containing protein 1
Q3UHD2	Gfod1	Glucose-fructose oxidoreductase domain-containing protein 1
Q9R0T8	Ikbke	Inhibitor of nuclear factor kappa-B kinase subunit epsilon
A2A7S8	Kiaa1522	Uncharacterized protein KIAA1522
O35071	Kif1c	Kinesin-like protein KIF1C
Q8C052	Map1s	Microtubule-associated protein 1S
Q60592	Mast2	Microtubule-associated serine/threonine-protein kinase 2
Q6PCP5	Mff	Mitochondrial fission factor
Q8R1S4	Mtss1	Metastasis suppressor protein 1
P28660	Nckap1	Nck-associated protein 1
Q9QYF9	Ndrg3	Protein NDRG3
P70313	Nos3	Nitric oxide synthase, endothelial
Q8CI95	Osbpl11	Oxysterol-binding protein-related protein 11
A2A8Z1	Osbpl9	Oxysterol-binding protein-related protein 9
Q3UEI1	Pde4c	cAMP-specific 3',5'-cyclic phosphodiesterase 4C
Q69Z38	Peak1	Pseudopodium-enriched atypical kinase 1
Q8BWJ3	Phka2	Phosphorylase b kinase regulatory subunit alpha, liver isoform
Q7TSH2	Phkb	Phosphorylase b kinase regulatory subunit beta
Q8K1N2	Phldb2	Pleckstrin homology-like domain family B member 2
Q4VAC9	Plekhg3	Pleckstrin homology domain-containing family G member 3
Q60953	Pml	Protein PML
A2AHG0	Prosapip1	ProSAP-interacting protein 1
A3KGS3	Ralgapa2	Ral GTPase-activating protein subunit alpha-2
Q8BQZ4	Ralgapb	Ral GTPase-activating protein subunit beta
O89032	Sh3pxd2a	SH3 and PX domain-containing protein 2A
O88343	Slc4a4	Electrogenic sodium bicarbonate cotransporter 1
Q99L88	Sntb1	Beta-1-syntrophin
P16546	Sptan1	Spectrin alpha chain, non-erythrocytic 1
Q9D0I4	Stx17	Syntaxin-17
Q8BJS4	Sun2	SUN domain-containing protein 2
Q5F2E8	Taok1	Serine/threonine-protein kinase TAO 1
Q9Z0U1	Tjp2	Tight junction protein ZO-2
Q9EP53	Tsc1	Hamartin
Q61037	Tsc2	Tuberin
P58854	Tubgcp3	Gamma-tubulin complex component 3
Q9QY76	Vapb	Vesicle-associated membrane protein-associated protein B
Q8BH57	Wdr48	WD repeat-containing protein 48
P83741	Wnk1	Serine/threonine-protein kinase WNK1
Q8VDZ4	Zdhhc5	Palmitoyltransferase ZDHHC5
Q9R049	Amfr	E3 ubiquitin-protein ligase AMFR
Q9DBT5	Ampd2	AMP deaminase 2
P62046	Lrch1	Leucine-rich repeat and calponin homology domain-containing protein 1
O08648	Map3k4	Mitogen-activated protein kinase kinase kinase 4
Q62433	Ndrg1	Protein NDRG1
P33215	Nedd1	Protein NEDD1
P62069	Usp46	Ubiquitin carboxyl-terminal hydrolase 46

95% probability) in which 157 proteins were enriched in the treated versus untreated samples (exp2). Comparing the two biological replicates, we identified 64 proteins that were enriched in both experiments (Fig. 1C), two of which are known AMPK substrates, ACC1 and TSC2 (Table 1).

3.2. Detection of AMPK-dependent targets

Given that the AMPK-activator mixture would produce some degree of off-target effects [22], we wanted to clarify whether the obtained hits were truly AMPK-dependent. We therefore analysed samples derived from hepatocytes genetically lacking both AMPKα-catalytic isoforms (AMPK KO). As anticipated [18,23], there was no detectable level of AMPKα proteins in AMPK KO hepatocytes, and most of the protein bands recognised by the phospho-AMPK motif antibody in the treated hepatocytes from control mice ($AMPK\alpha1^{lox/lox}\alpha2^{lox/lox}$) were absent in activator-treated AMPK KO samples (Fig. 1D). In the AMPK KO hepatocytes LC-MS/MS analysis identified 72 proteins which were enriched in the immunoprecipitates upon stimulation, whereas in the corresponding sample derived from control hepatocytes there were 157 enriched proteins, 125 of which were unique to the control sample (Fig. 1E). A large majority (89% or 57 out of 64 proteins) of the enriched proteins identified in the experiments using wild-type hepatocytes (exp1) were not enriched in the AMPK KO samples, confirming AMPK dependence (Table 1). In order to determine whether proteins enriched in the stimulated samples are likely targets/substrates of AMPK (as opposed to proteins co-immunoprecipitating with AMPK targets as binders), we performed bioinformatics analysis using PROSITE (http://prosite.expasy.org) [24] and screened our hits for the presence of the AMPK consensus L-X-R-X-X-*S/*T (X represents any amino acid and * denotes the phosphorylated residue) [16] which the phospho-AMPK motif antibody is raised against.

3.3. Biochemical validation of cingulin as an AMPK substrate

In our initial screen (exp1a–b) (Fig. 1A–C), MS analysis of tryptic peptides derived from phospho-AMPK motif antibody immunoprecipitates identified a phosphopeptide (SQ*SQASLTGLAFMSPSNR; * denotes phosphorylation) that displays a perfect match with AMPK consensus sequence (L-X-R-X-X-*S/*T) in the AICAR/A769662-treated samples (raw data not shown). This peptide is proteotypic to (i.e. a protein-specific sequence of) cingulin (residues 130–147 of mouse cingulin), a protein known to be localised at tight junctions which has also been shown to interact with microtubules in epithelial and endothelial cells [25]. Bioinformatic analysis showed that the phosphorylation site (S137 on human cingulin) and its surrounding residues (that conform to AMPK consensus) are well conserved in mammals and also in certain lower vertebrates like African clawed frog (*X. laevis*) (Fig. 2A). To validate one of the hits using an alternative method, we generated a phospho-specific cingulin (S137) antibody. The specificity of this antibody was confirmed by immunoblot analysis using extracts from COS-1 cells that had been transfected with constructs encoding FLAG-tagged wild-type or phospho-deficient S137A mutant of human cingulin (Fig. 2B). We also observed that the phospho-AMPK motif antibody recognised a band at the molecular weight of cingulin in the wild-type-expressing cells, which was ablated in extracts from the phospho-deficient S137A mutant-expressing cells (Fig. 2B). We then attempted to detect phosphorylation of endogenous S137 (S132 in mouse) phosphorylation of cingulin in primary hepatocytes. Our phospho-cingulin S137 antibody failed to detect a specific endogenous band either by direct immunoblotting or immunoblotting of total cingulin antibody immunoprecipitates of the extracts. We speculated that the antibody may not be sensitive enough to detect endogenous levels of phospho-cingulin, particularly in tissues where expression is low. Immunoblot analysis of a mouse tissue panel showed that cingulin expression in the liver was relatively low compared to the testis, pancreas and brain (Fig. 2C). We then screened several cell lines (data not shown) and found that cingulin was abundantly expressed in a human intestinal cell line (Caco2). Since we experienced that AICAR is relatively poor activator of AMPK in several of the immortalised cell lines we had tested, we stimulated Caco2 cells with a recently identified potent and selective AMPK activator (termed 991 or also named ex229) [26,27]. Phosphorylation of AMPK on Raptor was increased at 5 min and peaked at 30 min following the treatment, while ACC phosphorylation was readily saturated at 5 min. In contrast, phosphorylation of endogenous cingulin S137 was transiently (5–15 min) increased (~1.3–1.7-fold increase over untreated) and was returned to the resting level 30 min following compound treatment (Fig. 2D).

3.4. Tissue expression of MFF splice-variants and identification of in vivo phosphorylation sites on MFF by MS

We next wished to validate whether mitochondrial fission factor (MFF) is a genuine AMPK-dependent substrate. We were particularly interested in MFF, as AMPK is implicated in controlling energy metabolism

through modulating mitochondrial gene expression and functions [1] and also MFF-derived peptides were substantially enriched in the immunoprecipitates from the AICAR/A769662-treated samples. In the process of cloning MFF from murine RNA libraries (as described in the Materials and methods section), and as described previously [28], we noted the presence of multiple splice-variants with different expression profiles across mouse tissues (Fig. 3A). We therefore cloned three splice-variants from a mouse RNA library, which were the predominant variants in the liver (variant 1), testis (variant 2) and brain (variant 3) (Fig. 3B, Supplementary Fig. 1A and B). We found that splice variant 1 corresponds to XM_006496573.1 and variant 3 corresponds to NM_029409.2. In variant 2, amino acids 149–199 of NM_029409.2 were replaced with amino acids RRQNEIRYE.

To check the MFF variant expression and tissue distribution profile at the protein levels, a panel of mouse tissue lysates was immunoblotted using anti-MFF antibody (with or without prior immunoprecipitation with an anti-MFF antibody) (Fig. 3C). As a positive control, cell extracts (COS-1) that had been transfected with the coding region of the individual 3 variants were immunoblotted in parallel. We observed the presence of short variants (with gel mobility similar to the size of recombinant variant 1 protein) in most tissues, and a long variant in multiple tissues including the heart, muscle, brain, testis and liver. In the brain and muscle, we observed the largest variant, and some intermediate variant sizes were observed uniquely in testis (Fig. 3C). We were particularly interested in the short variant of MFF (variant 1) as it appeared to match the size of the predominant variant detected in multiple tissues including the liver. To determine which residues were phosphorylated in vivo (in intact cells), we overexpressed FLAG-MFF (variant 1) in COS-1 cells and affinity-purified recombinant MFF proteins were subjected to tryptic digestion followed by MS analysis for phospho-peptide mapping. We obtained sequence protein coverage of 81% and identified five phosphorylated sites (S48, S129, S131, S146 and S161) (Fig. 3D and Supplemental Fig. 1C). Among the identified phosphorylation sites, we noticed that two phosphorylation sites contain canonical AMPK phosphorylation motif, S129 on exon 3 (identical on all variants) and S146 at the very end of exon 3 (where the sequence immediately downstream of the serine depends on the splice variant) (Fig. 3B). More specifically, all variants contain basic residues (R) in −3 and hydrophobic residues (L) in −5 position, however only variant 1 (but not 2–3) contains a preferred hydrophobic residue (L) in +4 position.

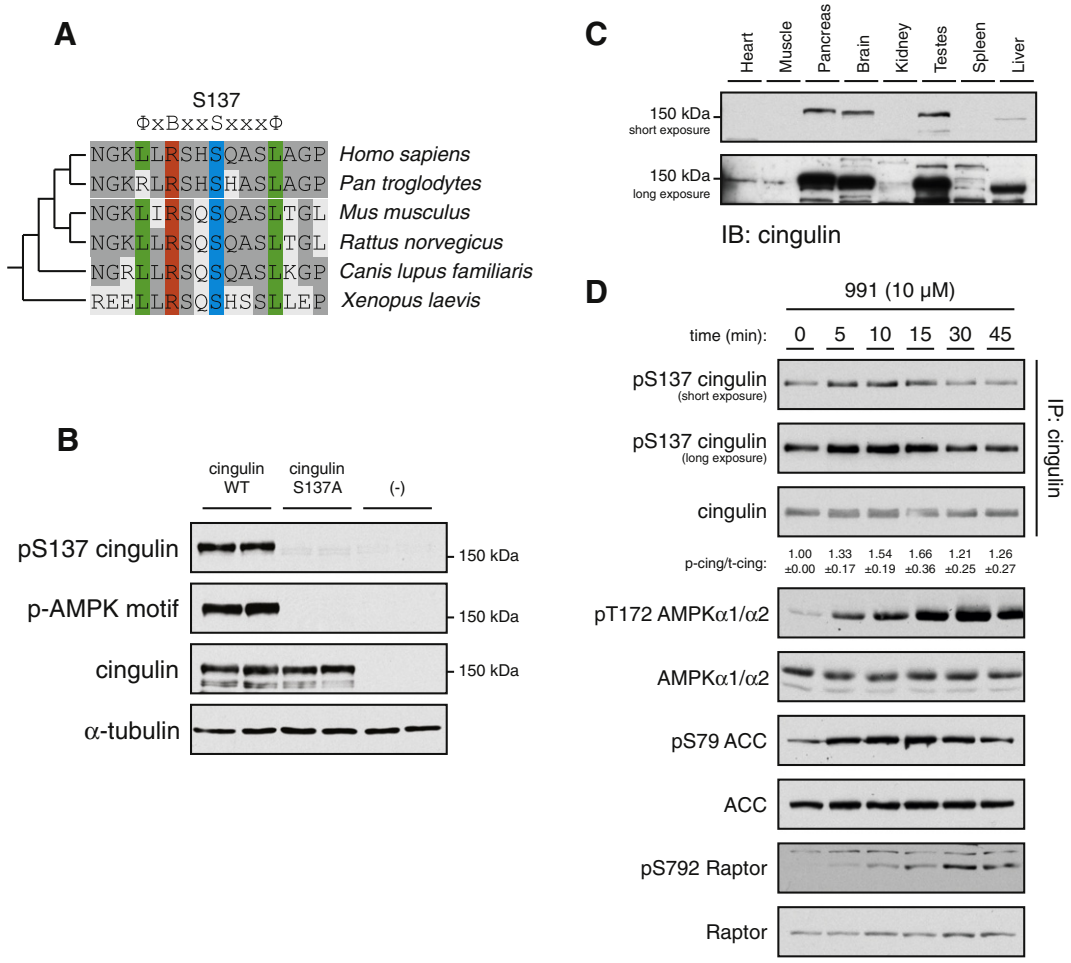

Fig. 2. Validation of cingulin as an AMPK substrate. (A) Sequences of cingulin from chimpanzee (XP_513800.2), mouse (NP_001032800.2), rat (XP_006232989.1), dog (NP_001096687.1) and clawed frog (NP_001081970.1) were aligned to the human sequence (NP_065821.1) using ClustalW (www.clustal.org). The region around pS137 of human is highlighted (grey: conserved residue compared to human; Φ: hydrophobic residue; B: basic residue). (B) COS-1 cells were transfected with wild-type and S137A-human cingulin or left untransfected. Cell lysates (10 μg) were analysed by immunoblotting using the indicated antibodies. (C) Tissue homogenates were prepared from organs harvested from C57BL/6 mice. Lysates (20 μg) were separated by SDS-PAGE and immunoblotted using anti-cingulin (Proteintech). Immunoblots are representative of two independent experiments. (D) Caco2 cells were treated with 10 μM 991 for the indicated times. Cingulin was immunoprecipitated from 200 μg of cell lysate with 1 μg anti-cingulin (Proteintech). Immunoprecipitates were separated by SDS-PAGE and immunoblotted using anti-pS137-cingulin and reprobed using anti-cingulin (Santa-Cruz). Immunoblots are representative of three independent experiments. The ratio of phospho- to total cingulin as measured by densitometry using Image Studio (LI-COR Biosciences) is indicated as mean ± standard error.

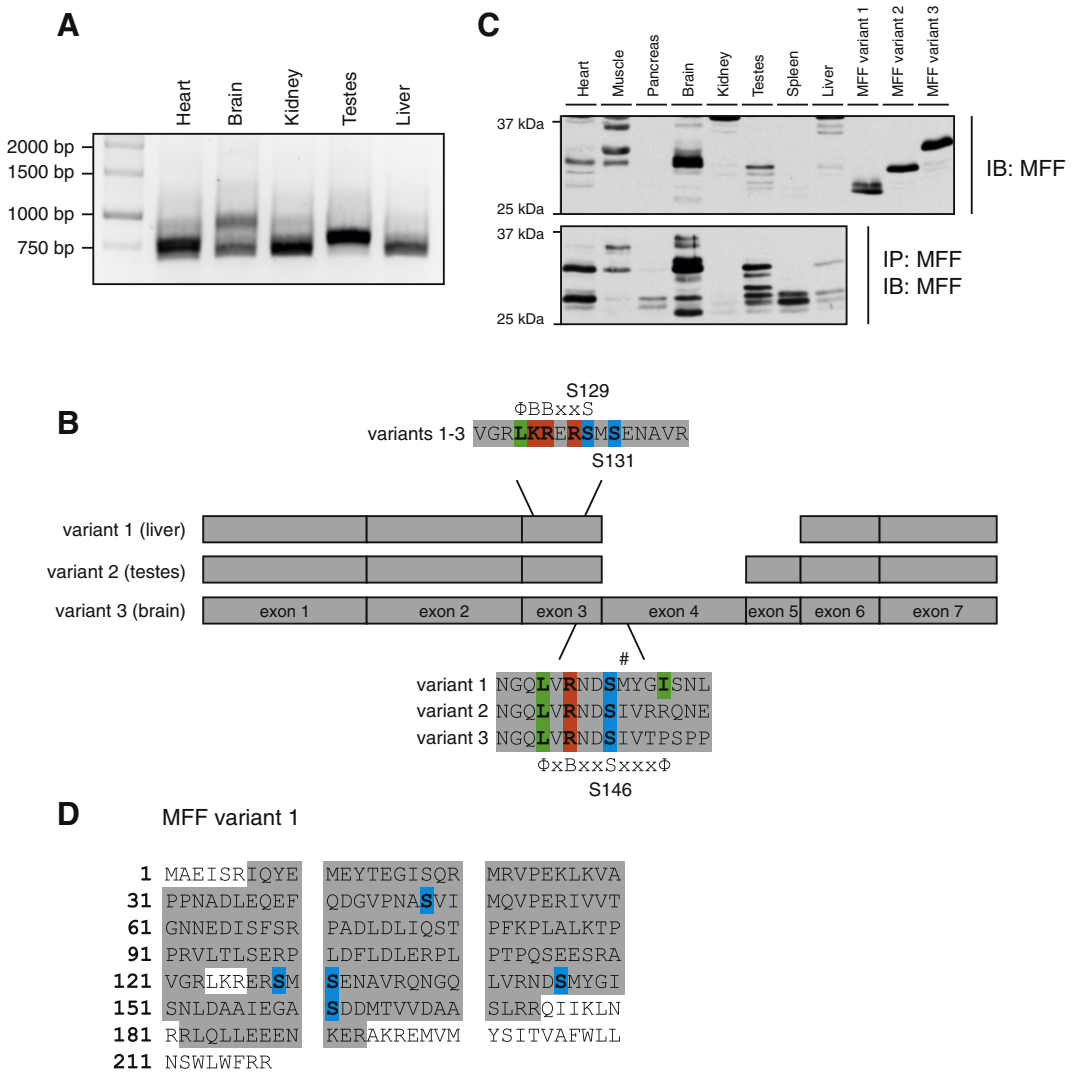

Fig. 3. Tissue expression of MFF splice-variants and determination of in vivo phosphorylation sites. (A) PCR amplification of the coding regions of MFF splice variants using 1 μg RNA from different tissues as a template and separation on agarose gel stained with SYBR Safe. The major PCR products of different tissues were cloned, the sequence verified, and further subcloned into expression vectors. (B) Comparison of the exon structure of the three MFF variants cloned from liver RNA (variant 1), testis RNA (variant 2) and brain RNA (variant 3). The regions around S129 and S146 (# indicates the splice junction site) correspond to the canonical AMPK phosphorylation motif (Φ: hydrophobic residue; B: basic residue). (C) MFF was immunoprecipitated from 200 μg of the indicated mouse tissue lysate with 1 μg anti-MFF (Santa Cruz). Lysates (40 μg, upper panel) and the immunoprecipitated proteins (lower panel) were separated by SDS-PAGE and immunoblotted using anti-MFF (Proteintech). COS-1 cell lysates (4 μg) overexpressing either one of the three cloned MFF variants were included as a control (molecular size reference). Immunoblots are representative of two independent experiments. (D) COS-1 cells were transfected with FLAG-MFF (variant 1) and cells were treated with 10 μM 991 for 30 min. MFF was immunoprecipitated using 5 μl FLAG-M2 resin. Immunoprecipitates were separated by SDS-PAGE and the gel was stained using colloidal Coomassie. Gel pieces containing MFF were excised for further processing (trypsin digestion and MS/MS analysis). Sequence coverage of 81% was obtained (grey shading) and 5 phosphorylated residues (S48, S129, S131, S146 and S161; blue shading) were detected (Supplementary Fig. 1C).

3.5. Overexpressed MFF was phosphorylated at S129 and S146 upon AMPK-activator treatment

To investigate the phosphorylation of MFF by AMPK, we generated phospho-specific antibodies designed to individually detect the candidate AMPK sites (S129 (variant 1–3) and S146 (variant 1)). We also generated another phospho-specific antibody against S131 (predicted not be regulated by AMPK based on surrounding peptide sequence) to demonstrate specificity of AMPK-dependent phosphorylation of S129 and/or S146 and also to address a concern that phosphorylation of S131 may interfere detection of S129 phosphorylation. To determine phospho-site-specificity of the antibodies, we ectopically expressed MFF (variant 1) (Fig. 3B) and phospho-deficient alanine mutants (S129A, S131A, S146A and all combinations thereof) in COS-1 cells (Fig. 4A) and immunoblot analysis of the extracts was performed. The pS146 antibody did not recognise any of the mutants where S146 was mutated to an alanine. On the other hand, both the pS129 and pS131 antibodies did not recognise MFF when either S129, S131 or both sites were mutated to an alanine, probably due to the proximity of the mutated residue to the phosphorylated serine affecting epitope recognition by the antibody and/or phosphorylation by the upstream kinase (Fig. 4A). The phospho-AMPK motif antibody recognised MFF with the S146A mutation, but not with the S129A mutation, suggesting that out of the two predicted AMPK motif sites (S129 and S146), phosphorylation of MFF at S129 is responsible for the immunoreactivity of MFF with the phospho-AMPK motif antibody (Fig. 4A).

Because the pS146 antibody was designed to recognise variant 1 in particular, we needed to verify its recognition of other variants. Overexpression of all three MFF variants and their S146A mutants in COS-1 cells showed that the antibody did not recognise variant 2, and only detected a weak signal from wild-type variant 3 (Fig. 4B). We also observed that variant 1, in contrast to variants 2 and 3, resolved as a doublet, and that the slower-migrating species disappeared in the S146A mutant (Fig. 4B). To examine if the doublet was indeed a consequence

of the phosphorylation event at S146, we immunoblotted purified FLAG-tagged MFF (wild-type and S146A mutant) pre-treated with or without λ-phosphatase. We observed that λ-phosphatase treatment resulted in the disappearance of the slower-migrating form of the doublet seen in wild-type MFF, indicating that phosphorylation at S146 is responsible for the band-shift (Fig. 4C). We next wanted to determine whether those phosphorylation sites were up-regulated upon AMPK activation in intact cells. The AMPK activator 991 robustly stimulated AMPK in COS-1 cells, as judged by phosphorylation of AMPKα and ACC (Fig. 4D). Treatment with 991 resulted in a modest increase in phosphorylation of S129 and S146, but not S131 sites in MFF (variant 1)-overexpressed COS-1 cells (Fig. 4D). The total MFF immunoblot revealed that even under treated conditions, the faster-migrating species of MFF was much more abundant than the slower-migrating species (phosphorylated at S146), indicating that the stoichiometry of phosphorylation at S146 is likely very low (Fig. 4D).

3.6. S129 phosphorylation and S146 phosphorylation of endogenous MFF were promoted upon AMPK activation

In order to study endogenous phosphorylation of MFF and its dependence on AMPK, we decided to return to the cell model used for MS analysis. Primary mouse hepatocytes were treated with the AMPK-activator mixture (AICAR/A769662), and MFF immunoprecipitates were subjected to immunoblotting using total and our phospho-specific MFF antibodies. We observed that three bands (presumably splice-variants) were present in primary hepatocytes as detected with the total MFF antibody (Fig. 5A), which corresponded with our liver protein expression profile (Fig. 3C). Upon AMPK stimulation, MFF phosphorylation at S129 was increased, whereas S131 phosphorylation was decreased in all three variants. The pS146 antibody recognised an increase in phosphorylation upon AMPK stimulation in the shorter variant of MFF. Together with the band-shift seen in

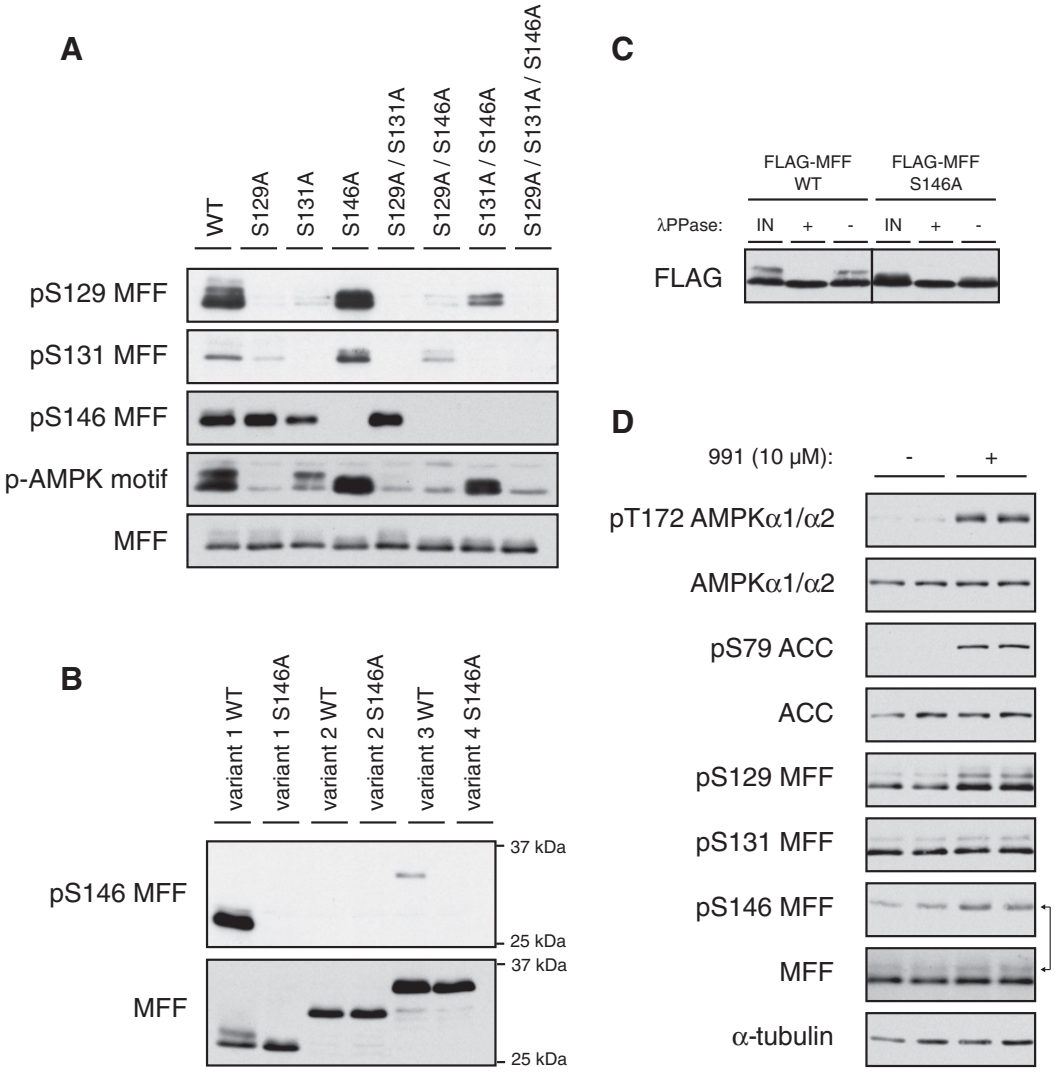

Fig. 4. MFF was phosphorylated at S129 and S146 upon AMPK activation in overexpressing COS-1 cells. (A) COS-1 cells were transfected with variant 1 of MFF (wild-type and non-phosphorylatable mutants as indicated). Cell extracts (10 μg) were analysed by immunoblotting using the indicated antibodies. Immunoblots are representative of two independent experiments. (B) COS-1 cells were transfected with variant 1, 2 or 3 of MFF or S146A mutants thereof. Cell extracts (10 μg) were separated by SDS-PAGE and immunoblotted using anti-pS146-MFF and anti-MFF (Proteintech). Immunoblots are representative of two independent experiments. (C) COS-1 cells were transfected with variant 1 of wild-type or S146A-MFF (FLAG-tagged). Total cell lysates (20 μg) were immunoprecipitated using FLAG-M2 resin. The immunoprecipitated proteins were then incubated at 30 °C for 30 min with (+) or without (−) λ-phosphatase as described in the Materials and methods section. Dephosphorylation reactions were terminated by boiling in Laemmli buffer and the resulting samples were separated by SDS-PAGE along with 20 μg total cell extracts (without λ-phosphatase) as reference input material (IN) and immunoblotted using anti-FLAG. Immunoblots are representative of 3 independent experiments. (D) COS-1 cells were transfected with variant 1 of MFF. Cells were then either left untreated or treated with 10 μM 991 for 30 min. Cell extracts (10 μg) were analysed by immunoblot analysis using the indicated antibodies. Immunoblots are representative of three independent experiments.

the shortest variant of MFF it is likely that this variant corresponds to variant 1 that we had cloned from mouse liver RNA (Fig. 3B). To determine if the regulation of phosphorylation on these three sites depends on activation of AMPK as opposed to an off-target effect of the compounds (AICAR/A769662), we assessed these phosphorylation events in AMPK KO hepatocytes. We observed that the up-regulation of S129 and S146, as well as the down-regulation of S131 phosphorylation in response to AICAR/A769662 treatment were substantially eliminated in the AMPK KO hepatocytes, confirming AMPK dependence of these phosphorylation events (Fig. 5B).

4. Discussion

In order to establish a methodology for identification of novel AMPK targets/substrates, we undertook an MS-based analysis of proteins/peptides that were isolated from hepatocyte extracts using a phospho-AMPK substrate motif antibody. We identified 57 proteins that were enriched in samples from hepatocytes treated with an AMPK-activator mixture (AICAR/A769662) (Table 1). AMPK dependence of the peptide enrichment/phosphorylation was established using AMPK KO hepatocytes, even though indirect modulation of phosphorylation (by other kinases/phosphatases) cannot be fully excluded. However, the presence of established AMPK phosphorylation motif(s) in the primary sequence enhances the likelihood that several of the identified proteins are direct AMPK targets. As shown in the current study, additional analyses to confirm endogenous phosphorylation of the hits in intact cells/tissues using phospho-specific antibodies (or alternative methods such as quantitative MS) and AMPK-deficient models with selective AMPK activators provide more comprehensive and reliable validation. Although our approach is straightforward and would be useful for identifying a large set of AMPK targets, there are some limitations. The phospho-AMPK substrate motif antibody is biased towards proteins/peptides harbouring the motif which was defined based on the kinase (purified AMPK) recognising short, linear peptides in vitro [14,16] and the antibody is raised against a degenerate peptide library containing fixed leucine and arginine residues at the −5 and −3 positions N-terminal to the phospho-acceptor (S/T) residue. Therefore, although the antibody may cross-react to some extent with peptides containing similar side chain properties (with leucine and arginine at the designated position), it is possible that only a subset of AMPK substrates that conform to this narrow recognition motif might be identified by this method. Structural modelling and site-directed mutagenesis have indicated additional determinants that, while not present in all previously identified substrates, improve the binding/kinetic parameters [12,14]. This may explain in part why our hit list contains only two known AMPK substrates (ACC1 and TSC2), although this may also be related to the relative abundance of known AMPK substrates in hepatocytes.

In our initial screen, we observed enrichment of a phosphopeptide (SQ*SQASLTGLAFMSPSNR) corresponding to residues 130-147of mouse cingulin that showed a perfect match with the AMPK consensus (L-X-R-X-X-*S/*T) in AMPK-activator-treated samples (data not shown). While we were validating AMPK-dependent cingulin phosphorylation (S137 on human cingulin) using a phospho-specific antibody, Yano et al. reported that cingulin is likely a novel AMPK substrate, and that AMPK-mediated phosphorylation of cingulin promotes association of planar apical microtubules with tight junctions [29]. Although the work was elegantly performed in terms of cell biology, evidence that AMPK phosphorylates cingulin was only derived from in vitro assay using recombinant preparations. Based on the sequence analysis of cingulin, they predicted that AMPK might phosphorylate S137 and S155 (equivalebt to S132 and S150 on mouse cingulin, respectively)) and they concluded that both sites might be phosphorylated by AMPK based on the finding that an in-gel detection of phosphoproteins (AMPK-phosphorylated cingulin) using fluorescent method in wild-type cingulin was abolished in the double S132A and S150A mutant, but not in the single mutant. We here provide evidence that endogenous cingulin S137 phosphorylation is transiently increased upon pharmacological AMPK activation in a human intestinal cell line (Caco2). This has validated our approach in characterizing the AMPK-

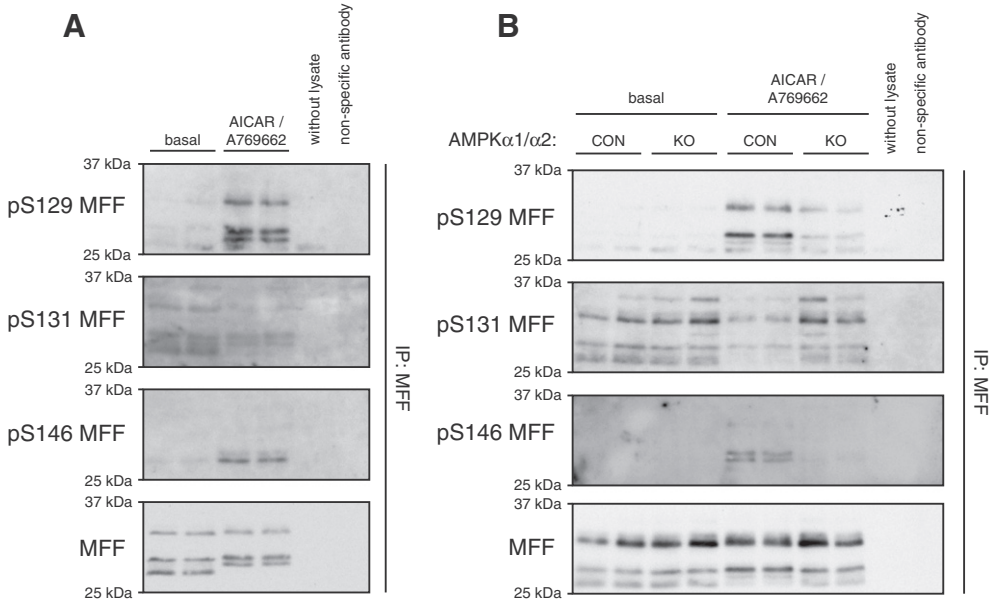

Fig. 5. S129 phosphorylation and S146 phosphorylation of endogenous MFF were up-regulated upon AMPK activation. (A) Primary hepatocytes were isolated from C57BL/6 mice (12-week-old). Plated cells were treated with vehicle or a combination of 0.3 mM AICAR and 10 μM A769662 for 45 min. Total cell lysates (500 μg) were immunoprecipitated using anti-MFF (Santa Cruz) or non-specific control antibody coupled to NHS-activated Sepharose. Immunoprecipitates were eluted by boiling in Laemmli buffer and the resulting samples were analysed by immunoblotting using the indicated antibodies. (B) Primary hepatocytes were isolated from AMPK KO and their control mice (CON) (10-week-old). Plated cells were treated with vehicle or a combination of 0.3 mM AICAR and 10 μM A769662 for 45 min. Total cell lysates (500 μg) were immunoprecipitated using anti-MFF (Santa-Cruz) or non-specific control antibody coupled to NHS-activated Sepharose. Immunoprecipitates were eluted by boiling in Laemmli buffer. Immunoprecipitated extracts were then separated by SDS-PAGE and immunoblotted using the indicated antibodies.

dependent phosphorylation site on cingulin, which complemented the functional analysis by Yano et al. [29]. Given that a phosphopeptide containing S150 of cingulin was not identified in our screen and the site does not appear to be a typical AMPK phosphorylation site (SNRST*S, *putative phosphorylation), we did not study this further. We noticed that a tight junction protein zonula occludens (ZO)-2, one of the tight junction proteins known to interact with cingulin [30], was also identified as a potential AMPK target (Table 1). ZO-2 contains a potential AMPK site (MRRAA*SRDQL, residue 955–964 of mouse ZO-2). It would be interesting to determine if ZO-2 is a direct substrate of AMPK or was identified merely by co-precipitation through direct interaction with cingulin.

AMPK is implicated in controlling cellular energy metabolism through modulating mitochondrial function. For example, AMPK activation has been reported to increase mitochondrial biogenesis through phosphorylating PGC-1α [31] or by increasing PGC-1α deacetylation via an increase in cellular NAD^+ content and SIRT1 activity [32]. AMPK has also been shown to regulate mitophagy via suppression of the mTOR pathway as well as directly phosphorylating ULK1 [33,34]. Furthermore, it has been reported that treatment of INS-1E pancreatic β-cells with AICAR protects mitochondria from palmitate-induced fragmentation via phosphorylation of Drp1 [35]. MFF is a mitochondrial outer membrane protein that has been proposed to play a role in the recruitment of Drp1 (which is a key player in mitochondrial division, during mitochondrial fission) [28,36,37]. Thus we were encouraged to investigate whether MFF is a cellular target of AMPK, as that may reveal a key role for AMPK in regulating mitochondrial function via controlling their dynamics of fission and fusion upon energy stress. We demonstrated that three splice-variants of endogenous MFF, present in primary mouse hepatocytes, were phosphorylated on S129. We also observed that the shortest variant (variant 1) was phosphorylated at an additional site (S146) upon AMPK activation. This might be due to the fact that variants 2–3 do not contain hydrophobic amino acid in the +4 position (from phospho-acceptor S146 site) (Fig. 3B) that is commonly seen in well-established AMPK substrates [12,15] and that also showed strong selectivity in a peptide library approach [16]. However, we cannot rule out the possibility that the pS146 antibody does not recognise phosphorylation of S146 in variants 2–3. It would be worthwhile examining if S146 is indeed phosphorylated and if so, whether it is increased in an AMPK-dependent mechanism. Whatever the case, it would be interesting to investigate the impact/role that AMPK-dependent phosphorylation of MFF plays (and also determine if there is a variant-specific role) on mitochondrial architecture and function. To this effect, one could study the effect of AMPK activation on mitochondrial morphology and whether expression of phospho-deficient MFF mutants in a cell system devoid of endogenous MFF (e.g. by knockout) affects Drp1 recruitment and ultimately fragmentation of the mitochondria.

5. Conclusions

We report a motif affinity proteomic approach for the discovery of cellular AMPK targets and validation of two specific hits of interest (cingulin and MFF). Although the method has some limitations (as described above in the Discussion section), by combining genetic models as well as specific AMPK activators, this approach can become a powerful and reliable screening method that enables researchers to identify a large set of potential AMPK targets in various cells/tissues.

Supplementary data to this article can be found online at http://dx.doi.org/10.1016/j.cellsig.2015.02.008.

Contribution statement

K.S. came up with the concept of the study and K.S., N.A.M. and S.D. designed the overall experiments.

S.D. performed all the immortalised cell experiments using COS-1, Caco2 and biochemical analyses (immunoblots, immunoprecipitation). Molecular biology (cloning, sequencing, mutagenesis, and RT-PCR (Fig. 3A)) was performed by M.D. R.F. and G.R.S. contributed to the preparations of mouse primary hepatocyte samples (Figs. 1A–C, 5A) and M.F. and B.V. generated AMPK KO mouse model and prepared hepatocytes for the analysis shown in Figs. 1D, E, and 5B. N.M., D.S., L.D., and A.N.G. performed mass spectrometry (MS) analysis and N.M., D.S., L.D., S.D., and K.S. contributed to bioinformatics analysis and interpretation of MS-related results. S.D. and K.S. drafted the manuscript and all other co-authors contributed and edited the draft.

Disclosure statement

The authors declare no conflict of interest associated with this study.

Acknowledgements

We thank the Functional Genomics at Nestlé Institute of Health Sciences (led by Patrick Descombes) for their support in DNA sequence analysis. We also thank Mathieu Membrez for Caco2 cell culture advice and Roger Hunter for critical reading of the manuscript (both at Nestlé Institute of Health Sciences). This work was supported by the Région Ile-de-France (CORDDIM) and the Société Francophone du Diabète (SFD). This work was also supported by grants to G.R.S. from the Canadian Institutes of Health Research (811812) and the Canadian Diabetes Association (846130). G.R.S. is a Canada Research Chair in Metabolism and Obesity and the McMaster University J Bruce Duncan Chair in Metabolic Diseases.

References

[1] D.G. Hardie, F.A. Ross, S.A. Hawley, Nat. Rev. Mol. Cell Biol. 13 (2012) 251–262.
[2] G.R. Steinberg, B.E. Kemp, Physiol. Rev. 89 (2009) 1025–1078.
[3] G.J. Gowans, D.G. Hardie, Biochem. Soc. Trans. 42 (2014) 71–75.
[4] J.S. Oakhill, R. Steel, Z.P. Chen, J.W. Scott, N. Ling, S. Tam, B.E. Kemp, Science 332 (2011) 1433–1435.
[5] B. Xiao, M.J. Sanders, E. Underwood, R. Heath, F.V. Mayer, D. Carmena, C. Jing, P.A. Walker, J.F. Eccleston, L.F. Haire, P. Saiu, S.A. Howell, R. Aasland, S.R. Martin, D. Carling, S.J. Gamblin, Nature 472 (2011) 230–233.
[6] D.R. Alessi, K. Sakamoto, J.R. Bayascas, Annu. Rev. Biochem. 75 (2006) 137–163.
[7] K. Sakamoto, O. Goransson, D.G. Hardie, D.R. Alessi, Am. J. Physiol. Endocrinol. Metab. 287 (2004) E310–E317.
[8] D.G. Hardie, K. Sakamoto, Physiology 21 (2006) 48–60.
[9] H.M. O'Neill, S.J. Maarbjerg, J.D. Crane, J. Jeppesen, S.B. Jorgensen, J.D. Schertzer, O. Shyroka, B. Kiens, B.J. van Denderen, M.A. Tarnopolsky, B.E. Kemp, E.A. Richter, G.R. Steinberg, Proc. Natl. Acad. Sci. U. S. A. 108 (2011) 16092–16097.
[10] K. Sakamoto, G.D. Holman, Am. J. Physiol. Endocrinol. Metab. 295 (2008) E29–E37.
[11] H.M. O'Neill, J.S. Lally, S. Galic, M. Thomas, P.D. Azizi, M.D. Fullerton, B.K. Smith, T. Pulinilkunnil, Z. Chen, M.C. Samaan, S.B. Jorgensen, J.R. Dyck, G.P. Holloway, T.J. Hawke, B.J. van Denderen, B.E. Kemp, G.R. Steinberg, Diabetologia 57 (2014) 1693–1702.
[12] D.G. Hardie, Genes Dev. 25 (2011) 1895–1908.
[13] S. Dale, W.A. Wilson, A.M. Edelman, D.G. Hardie, FEBS Lett. 361 (1995) 191–195.
[14] J.W. Scott, D.G. Norman, S.A. Hawley, L. Kontogiannis, D.G. Hardie, J. Mol. Biol. 317 (2002) 309–323.
[15] M.C. Towler, D.G. Hardie, Circ. Res. 100 (2007) 328–341.
[16] D.M. Gwinn, D.B. Shackelford, D.F. Egan, M.M. Mihaylova, A. Mery, D.S. Vasquez, B.E. Turk, R.J. Shaw, Mol. Cell 30 (2008) 214–226.
[17] O. Goransson, A. McBride, S.A. Hawley, F.A. Ross, N. Shpiro, M. Foretz, B. Viollet, D.G. Hardie, K. Sakamoto, J. Biol. Chem. 282 (2007) 32549–32560.
[18] M. Foretz, S. Hebrard, J. Leclerc, E. Zarrinpashneh, M. Soty, G. Mithieux, K. Sakamoto, F. Andreelli, B. Viollet, J. Clin. Invest. 120 (2010) 2355–2369.
[19] M.D. Fullerton, F. Hakimuddin, A. Bonen, M. Bakovic, J. Biol. Chem. 284 (2009) 25704–25713.
[20] K. Patel, M. Foretz, A. Marion, D.G. Campbell, R. Gourlay, N. Boudaba, E. Tournier, P. Titchenell, M. Peggie, M. Deak, M. Wan, K.H. Kaestner, O. Goransson, B. Viollet, N.S. Gray, M.J. Birnbaum, C. Sutherland, K. Sakamoto, Nat. Commun. 5 (2014) 4535.
[21] S. Ducommun, R.J. Ford, L. Bultot, M. Deak, L. Bertrand, B.E. Kemp, G.R. Steinberg, K. Sakamoto, Am. J. Physiol. Endocrinol. Metab. 306 (2014) E688–E696.
[22] B. Guigas, K. Sakamoto, N. Taleux, S.M. Reyna, N. Musi, B. Viollet, L. Hue, IUBMB Life 61 (2009) 18–26.
[23] R.W. Hunter, M. Foretz, L. Bultot, M.D. Fullerton, M. Deak, F.A. Ross, S.A. Hawley, N. Shpiro, B. Viollet, D. Barron, B.E. Kemp, G.R. Steinberg, D.G. Hardie, K. Sakamoto, Chem. Biol. 21 (2014) 866–879.

[24] C.J. Sigrist, L. Cerutti, N. Hulo, A. Gattiker, L. Falquet, M. Pagni, A. Bairoch, P. Bucher, Brief. Bioinform. 3 (2002) 265–274.
[25] C.M. Van Itallie, J.M. Anderson, Semin. Cell Dev. Biol. 36C (2014) 157–165.
[26] B. Xiao, M.J. Sanders, D. Carmena, N.J. Bright, L.F. Haire, E. Underwood, B.R. Patel, R.B. Heath, P.A. Walker, S. Hallen, F. Giordanetto, S.R. Martin, D. Carling, S.J. Gamblin, Nat. Commun. 4 (2013) 3017.
[27] Y.C. Lai, S. Kviklyte, D. Vertommen, L. Lantier, M. Foretz, B. Viollet, S. Hallen, M.H. Rider, Biochem. J. 460 (2014) 363–375.
[28] S. Gandre-Babbe, A.M. van der Bliek, Mol. Biol. Cell 19 (2008) 2402–2412.
[29] T. Yano, T. Matsui, A. Tamura, M. Uji, S. Tsukita, J. Cell Biol. 203 (2013) 605–614.
[30] M. Cordenonsi, F. D'Atri, E. Hammar, D.A. Parry, J. Kendrick-Jones, D. Shore, S. Citi, J. Cell Biol. 147 (1999) 1569–1582.
[31] S. Jager, C. Handschin, J. St-Pierre, B.M. Spiegelman, Proc. Natl. Acad. Sci. U. S. A. 104 (2007) 12017–12022.
[32] C. Canto, L.Q. Jiang, A.S. Deshmukh, C. Mataki, A. Coste, M. Lagouge, J.R. Zierath, J. Auwerx, Cell Metab. 11 (2010) 213–219.
[33] D.F. Egan, D.B. Shackelford, M.M. Mihaylova, S. Gelino, R.A. Kohnz, W. Mair, D.S. Vasquez, A. Joshi, D.M. Gwinn, R. Taylor, J.M. Asara, J. Fitzpatrick, A. Dillin, B. Viollet, M. Kundu, M. Hansen, R.J. Shaw, Science 331 (2011) 456–461.
[34] J. Kim, M. Kundu, B. Viollet, K.L. Guan, Nat. Cell Biol. 13 (2011) 132–141.
[35] J.D. Wikstrom, T. Israeli, E. Bachar-Wikstrom, A. Swisa, Y. Ariav, M. Waiss, D. Kaganovich, Y. Dor, E. Cerasi, G. Leibowitz, Mol. Endocrinol. 27 (2013) 1706–1723.
[36] O.C. Loson, Z. Song, H. Chen, D.C. Chan, Mol. Biol. Cell 24 (2013) 659–667.
[37] H. Otera, C. Wang, M.M. Cleland, K. Setoguchi, S. Yokota, R.J. Youle, K. Mihara, J. Cell Biol. 191 (2010) 1141–1158.